CHAPTER 4

Reduction of unusual iron-sulfur clusters in the H_2-sensing regulatory Ni-Fe hydrogenase from *Ralstonia eutropha* H16

Thorsten Buhrke[1$], Simone Löscher[2$], Oliver Lenz[1], Eberhard Schlodder[3], Ingo Zebger[3], Lars K. Andersen[3], Peter Hildebrandt[3], Wolfram Meyer-Klaucke[4], Holger Dau[2], Bärbel Friedrich[1], and Michael Haumann[2]

[1]Humboldt-Universität zu Berlin, Institut für Biologie/Mikrobiologie, Chausseestr. 117, D-10115 Berlin, Germany; [2]Freie Universität Berlin, FB Physik, Arnimallee 14, D-14195 Berlin, Germany; [3]Technische Universität Berlin, Institut für Chemie, Max-Volmer-Laboratorium für Biophysikalische Chemie, Sekr. PC14, Straße des 17. Juni 135, D-10623 Berlin, Germany; [4]DESY, EMBL Outstation, Notkestr. 85, D-22603 Hamburg, Germany.

Published in *J. Biol. Chem.* 280 (2005) 19488-19495

[$] Thorsten Buhrke and Simone Löscher contributed equally to this work.

Keywords:
Bioinorganic chemistry, Ni-Fe hydrogenase, hydrogen sensor, Fe-S clusters, X-ray absorption spectroscopy.

Abbreviations: EPR, electron paramagnetic resonance spectroscopy; EXAFS, extended X-ray absorption fine structure; Fe, iron; FTIR, Fourier-transform infrared spectroscopy; Ni, nickel; RH, regulatory Ni-Fe hydrogenase; RH^{+H_2}, H_2-flushed RH; RH^{ox}, air-oxidized RH; XANES, X-ray absorption near-edge structure; XAS, X-ray absorption spectroscopy.

Acknowledgements
We thank the staff at the EMBL Outstation Hamburg for excellent support, Prof. R. Bittl and Dr. C. Kay (FU Berlin) for generous help with the EPR experiments, Prof. S. Albracht (Amsterdam) for helpful advice in the FTIR experiments, Dr. K. Irrgang (Technische Universität Berlin) for kind support in AAS, and J. Stöhr for excellent technical assistance. We are indebted to Dr. H. Stosnach from Röntec (Berlin) for generous support in the TXRF measurements.

This work was supported by Deutsche Forschungsgemeinschaft Grant SFB 498 (Projects C1, C6, C8, and A8) and by the Fonds der Chemischen Industrie. The costs of publication of this article were defrayed in part by the payment of page charges. This article must therefore be hereby marked "*advertisement*" in accordance with 18 U.S.C. Section 1734 solely to indicate this fact.

Abstract

The regulatory Ni-Fe hydrogenase (RH) from *Ralstonia eutropha* functions as a hydrogen sensor. The RH consists of the large subunit HoxC housing the Ni-Fe active site and the small subunit HoxB containing Fe-S clusters. The heterolytic cleavage of H2 at the Ni-Fe active site leads to the EPR-detectable Ni-C state of the protein. For the first time, the simultaneous but EPRinvisible reduction of Fe-S clusters during Ni-C state formation was demonstrated by changes in the UV-visible absorption spectrum as well as by shifts of the iron K-edge from x-ray absorption spectroscopy in the wildtype double dimeric RHWT [HoxBC]2 and in a monodimeric derivative designated RHstop lacking the C-terminal 55 amino acids of HoxB. According to the analysis of iron EXAFS spectra, the Fe-S clusters of HoxB pronouncedly differ from the three Fe-S clusters in the small subunits of crystallized standard Ni-Fe hydrogenases. Each HoxBC unit of RHWT seems to harbour two [2Fe-2S] clusters in addition to a 4Fe species, which may be a [4Fe-3S-3O] cluster. The additional 4Fe-cluster was absent in RHstop. Reduction of Fe-S clusters in the hydrogen sensor RH may be a first step in the signal transduction chain, which involves complex formation between [HoxBC]2 and tetrameric HoxJ protein, leading to the expression of the energy converting Ni-Fe hydrogenases in *R. eutropha*.

Introduction

Ni-Fe hydrogenases represent an important class of metalloenzymes which catalyse the reversible cleavage of molecular hydrogen into electrons and protons (reaction $H_2 \Leftrightarrow 2H^+ + 2e^-$) (1). The chemolithoautotrophic β-proteobacterium bacterium *Ralstonia eutropha* H16 houses three different Ni-Fe hydrogenases which are physiologically active in the presence of O_2 (2,3). The membrane-bound (MBH) and soluble NAD-reducing (SH) enzymes are involved in energy conversion (4,5).

The regulatory Ni-Fe hydrogenase (RH) belongs to a particularly interesting type of Ni-Fe hydrogenases functioning as hydrogen sensors (6). Hydrogen sensors have also been described in *Bradyrhizobium japonicum* (7) and *Rhodobacter capsulatus* (8). Upon the interaction of the RH with molecular hydrogen, a complex signal transduction cascade is initiated which leads to the expression of the energy converting hydrogenases (9).

The RH consists of the large subunit HoxC that harbors the hydrogen-activating Ni-Fe site and the small subunit HoxB that contains iron sulfur clusters (6). Several unusual properties of the RH (3,10,11) are remarkably different from those of the so-called standard Ni-Fe hydrogenases from, i.a., *Desulfovibrio gigas* and *Allochromatium vinosum* (1,12,13). In contrast to the dimeric standard Ni-Fe hydrogenases the RH forms a double dimer $[HoxBC]_2$ (Fig. 1A) which is connected to a tetramer of the HoxJ protein (14). The N-terminal input module of HoxJ containing a PAS domain is required for the formation of the RH-HoxJ complex whereas the C-terminal domain of HoxJ has histidine protein kinase activity (14). The RH cleaves H_2 only at extremely low rates (3,10). In contrast to standard hydrogenases which can exist in up to nine different redox states (1,13), in the RH only two states of functional relevance have been

detected (10). After aerobic isolation the enzyme is in its oxidized state containing Ni^{II}. This state does not need to be activated, but is always ready to bind hydrogen, a prerequisite for the sensor function (10,11). In the presence of H_2 it is rapidly converted to a state revealing a typical EPR-signal, termed Ni-C, due to a Ni^{III}-H^- species formed during heterolytic H_2-cleavage (15). In standard Ni-Fe hydrogenases the Ni is coordinated by four conserved cysteine residues. X-ray absorption spectroscopy (XAS) investigations on the RH, however, revealed that Ni may be coordinated by less than four cysteines (11). The Fe atom of the RH active site, on the other hand, carries two cyanides and one CO molecule, similar to standard Ni-Fe hydrogenases (3,10).

Although information has become available about the sequence of events that occur at the Ni-Fe active site upon interaction of the RH with H_2 (10,11,15), it is unclear whether electron transfer out of the Ni-Fe site takes place during H_2-cleavage and where these electrons are transferred to. Information on these points is expected to contribute to the understanding of the H_2-sensing mechanism of the RH-HoxJ complex (14).

In standard Ni-Fe hydrogenases of the *D. gigas* type, the small subunit contains three Fe-S clusters, two [4Fe-4S] and one [3Fe-4S] (16), which are bound via conserved cysteines and one histidine residue found in all Ni-Fe hydrogenase sequences. During hydrogen turnover these clusters become reduced as detected by EPR spectroscopy (1,17). The RH small subunit HoxB also contains these conserved cysteines. Therefore, it was postulated that it might also harbor three Fe-S clusters (6). EPR investigation of the RH, however, did not show reduced Fe-S clusters when the Ni-C EPR signal was formed under H_2 (3,10,15). It has been proposed that a non-Fe-S cofactor may be involved in electron transfer instead (10).

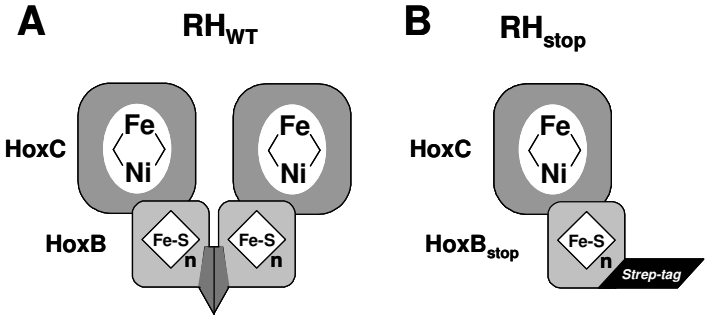

Figure 1: Schematic representation of the subunit compositions of (A) RH_{WT} and (B) RH_{stop}.

In this work, the double dimeric wild-type RH (RH_{WT}, Fig. 1A) and a derivative denoted as RH_{stop} (Fig. 1B) which forms a monodimer due to mutational truncation of the C-terminus of HoxB (14) were compared. It has been suggested that the RH_{stop} may lack the putative non-Fe-S cofactor (14). In both preparations, for the first time reduction of Fe-S clusters in the presence of H_2 was clearly detected in UV-VIS spectra and by X-ray absorption spectroscopy (XAS) at the Fe K-edge. Support for reduction of a non-Fe-S cofactor was not obtained. Seemingly, the Fe-S clusters of the RH differ from those of standard hydrogenases.

Materials and Methods

Bacteria growth and enzyme purification

Strains with the initials HF were derived from *R. eutropha* H16 (DSM428, ATCC 17699). Large-scale cultivation of *R. eutropha* strains, cell harvesting, cell disruption and preparation of soluble protein extracts were published before (10,14). RH_{WT} (Fig. 1A) was purified from the RH-overproducing strain *R. eutropha* HF371(pGE378) as described in (10). Starting with 50 g of cells (wet weight) yielded 3.7 mg of RH with a specific activity of 1.6 units/mg of protein. The RH_{stop} protein (Fig. 1B) was purified from *R. eutropha* HF574(pGE567) as a Strep-tag II fusion protein (Buhrke *et al*. 2005). Starting with 18 g of cells yielded 1.5 mg of RH_{stop} with a specific activity of 1.6 units/mg of protein.

The homogeneity of the respective protein preparations was investigated by SDS-PAGE analysis and subsequent Coomassie staining. The amount of impurities was quantified by using the Gelscan Professional V5.1 software (BioSciTec, Frankfurt, Germany). After background substraction, the sum of the % DID (differential integrated density) of the HoxC- and HoxB-specific bands was correlated to the sum of the % DID from the contaminating proteins.

Assays of hydrogenase activity

H_2-oxidizing activity was quantified by an amperometric H_2 uptake assay as in (3) using a H_2-electrode with methylene blue as an electron acceptor. One unit of H_2-methylene blue oxidoreductase activity was the amount of enzyme which catalyzed the consumption of 1 µmol H_2 per min. Protein concentrations were determined according to the protocol of Bradford (18).

Analysis of metal contents

Atomic absorption spectroscopy (AAS) and total reflection X-ray fluorescence analysis (TXRF) (19) was used for quantification of Ni and Fe. For AAS, three aliquots of each RH preparation were solubilized over night in concentrated HNO_3 (65 %, Suprapur, Merck), then diluted with ultrapure water (Millipore) to 1-5 % HNO_3, and further diluted for measurements using the transversely heated graphite furnace (THGA) technique with longitudinal Zeeman-effect background correction on a Perkin Elmer Aanalyst 800 spectrometer equipped with an autosampler and WinLab32 software in the laboratory of Dr. Klaus Irrgang (TU-Berlin). TXRF for simultaneous Ni and Fe quantification was performed on a Picotax spectrometer at Röntec (Berlin, Germany) using 1 µl of concentrated and dried protein solutions. Ni and Fe contents were determined against commercial Ni and Fe standards (Fluka) in AAS and relative to a Ga standard in TXRF.

Fourier-transform infrared spectroscopy (FTIR)

FTIR measurements were carried out with a Bruker IFS66V/S spectrometer equipped with a photovoltaic MCT detector, using a resolution of 2 cm^{-1}. The sample compartment was purged with nitrogen. Samples were held in a temperature-controlled (23 °C) gas-tight liquid cell (volume ~7 µl) with CaF_2 windows. FTIR spectra were baseline corrected using the software available with the spectrometer.

EPR spectroscopy

EPR measurements were performed in the laboratory of Prof. Robert Bittl (FU-Berlin) on an X-band Bruker Elexsys E580 spectrometer equipped with a SHQE resonator and a helium cryostat (Oxford) (microwave frequency of 9.6 GHz). For further conditions see figure legends. From each enzyme spectrum, the background from sample holder and cavity was subtracted. EPR signals in enzyme samples were quantified by comparison with the integrated intensities of signals from $CuSO_4$ solutions used as spin standards (20).

UV-VIS spectroscopy

Purified samples of wild-type RH and RH_{stop} were diluted with 20 mM Tris-HCl (pH 8.0) to a protein concentration of 0.64 mg/mL. UV-VIS spectra were recorded on a Cary 1E spectrophotometer (Varian) with a spectral resolution of 0.3 nm. To reduce the RH samples, protein solutions were flushed with hydrogen gas for 1 min. Subsequently, the sample was centrifuged (1 min, 12000 x g) to remove small amounts of precipitated protein. The clear supernatant was immediately re-transferred to the cuvette and the UV-VIS spectrum of the reduced sample was recorded.

X-ray absorption spectroscopy (XAS)

X-ray absorption spectra at the iron K-edge were collected at beamline D2 of the EMBL at HASYLAB (DESY, Hamburg, Germany). XAS samples contained 10-20 µL of RH solution (protein concentration 0.4-1 mM). Fluorescence-detected XAS spectra were measured with a 13-element solid-state Germanium detector (Canberra) at 20 K as described elsewhere (11). An absolute energy calibration (accuracy ±0.1 eV) was performed by monitoring the Bragg reflections of a crystal positioned at the end of the beamline (21). 3 scans of ~60 min duration were taken on the same spot (4.5 x 1 mm) of the sample. Comparison of the first and third scan revealed that radiation damage to the samples was absent because the Fe K-edge energy remained unchanged. Six scans, obtained on two separate spots of the samples, were averaged for each EXAFS spectrum. Spectra were normalized and EXAFS oscillations were extracted as in (22). The energy scale of Fe EXAFS spectra was converted to a *k*-scale using an E_0 of 7112 eV; E_0 refined to 7120 eV during the EXAFS simulations. Unfiltered k^3-weighted spectra were used for least-squares curve-fitting (22) and for calculation of Fourier-

transforms representing *k*-values ranging from 1.85 to 13 $Å^{-1}$. The data was multiplied by a fractional cosine window (10 % at low and high *k*-side). For EXAFS simulations, complex backscattering amplitudes were calculated using FEFF 7 (23); the amplitude reduction factor S_0^2 was 0.9. For XAS sample preparation, RH solutions were three times degassed under vacuum and subsequently flushed for 10 min with H_2 gas. As isolated and H_2-reduced samples were filled under argon or H_2 atmosphere into Kapton-covered acrylic glass sample holders using syringes previously filled with Ar or H_2. The same samples were used for EPR (prior to and after XAS) and XAS measurements.

Results

Comparison of the Ni-Fe active site in RH_{WT} and RH_{stop}

To test whether truncation of the C-terminal 55 amino acids of HoxB affected the Ni-Fe site, preparations of RH_{WT} and RH_{stop} were examined by FTIR and EPR measurements. The FTIR spectrum of oxidized RH_{stop} was identical to that of RH_{WT} (Fig. 2A) in showing an intense peak at 1942 cm^{-1} originating from the Fe-CO and two peaks at 2072 cm^{-1} and 2081 cm^{-1} from the two Fe-CN stretching vibrations as previously reported (3,10). Upon reduction of the samples by H_2, the υ(CO) vibration in both spectra shifted to higher frequencies by 18.5 cm^{-1} (not shown) whereas the υ(CN) vibrations remained unaffected as previously observed for RH_{WT} (10).

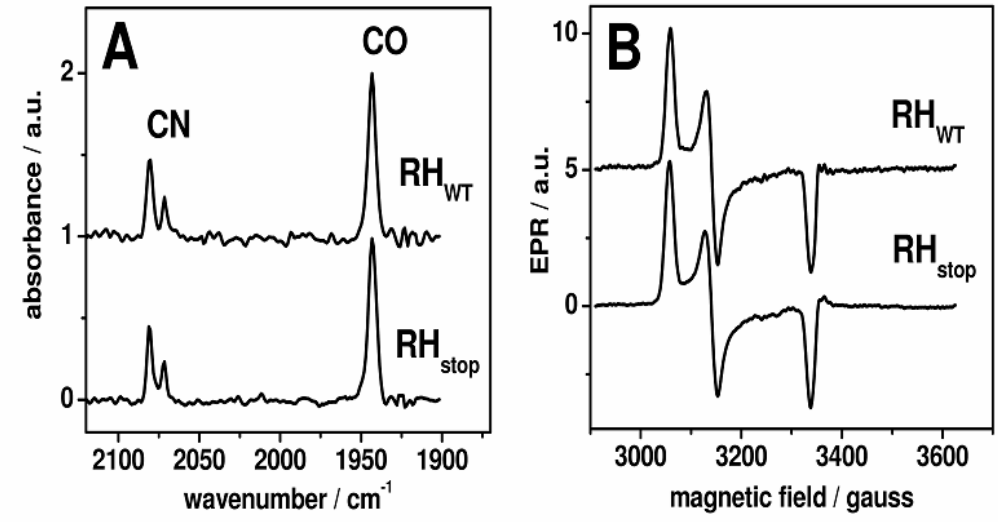

Figure 2: (A) FTIR spectra of oxidized RH_{WT} and RH_{stop} (normalized on the CO-bands). (B) Normalized Ni-C EPR spectra due to Ni^{III}-H^- (15) in the H_2-reduced samples later used for XAS. EPR conditions: temperature 30 K, microwave power 250 µW, modulation amplitude/ frequency 2mT/ 100 KHz. Quantification of measured Ni-C spectra in combination with Ni determination by AAS revealed that >90 % of the Ni was present as Ni^{III} in RH_{WT} and RH_{stop}.

The redox properties of the Ni-Fe active site of RH_{stop} also turned out to be similar to those of RH_{WT} as detected by EPR (Fig. 2B). Flushing of the RH with H_2 generates the Ni-C state (Ni^{III}-H^-) of the Ni-Fe active site with the hydride in a bridging position between Ni and Fe (15). The Ni-C EPR signals (Fig. 2B) were similar in RH_{WT} and RH_{stop}. Signal quantification revealed that more than 90 % of the Ni was converted to Ni^{III} in both preparations after incubation with H_2 for 10 min, implying similarly effective heterolytic hydrogen cleavage. However, EPR signals from singly reduced Fe-S clusters were completely absent in the Ni-C state. Reduced Fe-S clusters were also not detected when temperatures between 6 and 50 K and microwave power variations between 0.01 and 10 mW were applied (data not shown).

In summary, RH_{WT} and RH_{stop} appeared to be similar with respect to the coordination of the Fe of the Ni-Fe site both in the oxidized state and in the Ni-C state which was near quantitatively formed in both cases in the presence of hydrogen. Moreover, both preparations showed identical hydrogenase activities (see Materials and Methods). The catalytic properties of RH_{stop} were thus not affected by the truncation of the C-terminus of HoxB.

Determination of metal contents

Analysis of the Ni contents by AAS in combination with protein determination yielded on the average about 0.6 Ni in the RH_{WT} and close to one Ni in the RH_{stop} (Table 1). The relatively low Ni content in RH_{WT} can be explained with impurities in the preparations. SDS-PAGE analysis indicated that preparations of RH_{WT} contained sizable amounts of copurified proteins whereas preparations of RH_{stop} were homogenous (Fig. 3). The amount of impurites in the RH_{WT} sample was quantified by calculating the intensities of HoxC- and HoxB-specific protein bands and the sum of the band intensities derived from the contaminating proteins. According to this analysis the RH_{WT} sample contained about 16 % of impurities while the RH_{stop} sample was pure. Therefore, assuming that each HoxBC unit of RH_{WT} also contained one Ni similar to RH_{stop}, it was estimated from the Fe/Ni ratios (Table 1) determined by two independent techniques (AAS and TXRF) that each HoxBC unit of RH_{WT} contained about 8-9 Fe, in accordance with previous estimates (10). The Fe content of RH_{stop} was about 4-6 and thus distinctly lower than that of RH_{WT}.

Table 1: Metal contents of RH preparations.

	Ni / [HoxBC]	Fe / [HoxBC]	Fe / Ni
RH_{WT}	0.55±0.15	6.7±2.3	7.9±0.7
RH_{stop}	1.02±0.26	4.9±2.8	4.9±1.8

Fe,Ni/[HoxBC] values represent the average over values from AAS and protein determinations $(C_{Fe,Ni}/C_{[HoxBC]})^{mean}$ from four independent preparations of RH_{WT} and RH_{stop}. Mean Fe/Ni ratios were derived from the AAS values and from concentrations determined by TXRF on two preparations of both RH_{WT} and RH_{stop}. The respective error ranges represent standard deviations ($\sigma^{1/2}$).

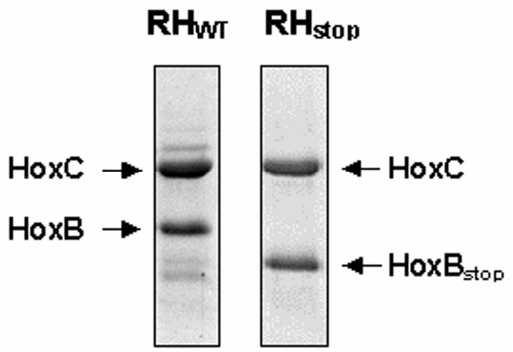

Figure 3: SDS-PAGE analysis of purified RH samples. Purified samples of RH_{WT} (left lane) and RH_{stop} (right lane) were separated by SDS polyacrylamide gel electrophoresis (12 % gels; 5 µg of protein per lane) and subsequently stained with Coomassie brilliant blue (Serva). The RH subunits HoxC and HoxB are indicated by arrows. Due to the truncation of its C-terminal 55 amino acids, the $HoxB_{stop}$ band from the RH_{stop} sample is found at a lower molecular weight than the native HoxB from the RH_{WT} sample.

Based on sequence homologies (see Discussion) one would expect HoxB to contain three [4Fe-4S] clusters (6). Taking also the Fe atom of the Ni-Fe site into account, one HoxBC monodimer might contain 13 Fe/Ni. Thus, the experimentally determined Fe content of RH_{WT} was significantly lower than expected. Furthermore, $HoxB_{WT}$ seemed to contain more Fe than $HoxB_{stop}$. The double dimeric RH_{WT} may thus comprise Fe-species which are absent in monodimeric RH_{stop}.

Detection of Fe-S cluster reduction by UV-VIS spectroscopy

The optical absorption spectra of the oxidized RH_{WT} and RH_{stop} showed, in addition to a peak at 280 nm due to the absorption of the aromatic amino acid residues of the protein, a broad shoulder around 410 nm presumably due to the presence of Fe-S clusters (Fig. 4, solid lines). That both preparations were fully oxidized was apparent from the absence of any Ni-C EPR signal (data not shown). The extinction coefficients were calculated at 390 nm and at 420 nm and compared to data from the literature (Table 2). The ε(420 nm) value determined for RH_{stop} is in good agreement with the value that would be expected in the presence of two cysteinyl-coordinated [2Fe-2S] clusters (49). The ε(420 nm) of RH_{WT}, on the other hand, is significantly higher, confirming the data from the metal analysis which indicate that RH_{WT} contain additional Fe species (see above). The ε(390 nm) values estimated for RH_{WT} as well as for RH_{stop} were significantly larger than the value of ε(390 nm) that was expected if only one [4Fe-4S] cluster was present (Table 2).

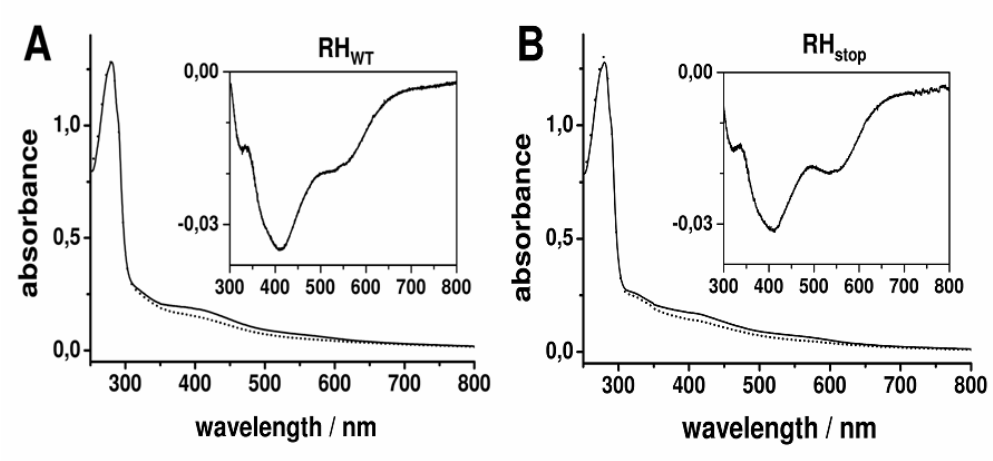

Figure 4: UV-VIS spectra of (A) RH_{WT} and (B) RH_{stop} (solid lines, oxidized; dotted lines, H_2-reduced). The insets show the difference of spectra (H_2-reduced minus oxidized).

When the RH was reduced by flushing of samples with H_2, increased absorption was observed in the whole spectral range (not shown); the curvature of the background (proportional to λ^{-4}) suggested its origin from a scattering contribution. Because this background could be removed by centrifugation of H_2-flushed samples, apparently a small portion of the RH protein precipitated to yield scattering aggregates. Aggregation was also observed after flushing with argon which indicated that it was not specifically caused by H_2.

Table 2: Extinction coefficients of preparations of RH_{WT} and RH_{stop} at 390 nm and at 420 nm as obtained from the UV-VIS spectra (Fig. 4).

	ε(390 nm) [M^{-1} cm^{-1}]	ε(420 nm) [M^{-1} cm^{-1}]
RH_{WT}^{ox} *(a)*	31500	28300
RH_{stop}^{ox}	23900	21800
[4Fe-4S]	15200*(b)*	
2 x [2Fe-2S]		19200*(b)*

(a) The values for RH_{WT} were corrected by a factor of 1.188 due to the fact that preparations of RH_{WT} contained 16 % impurities. *(b)* These values were taken from (49).

Reduction of RH_{WT} by flushing with H_2 and subsequent removal of aggregates by centrifugation yielded a spectrum with clearly decreased absorption between 350 and 600 nm compared to the oxidized state (Fig. 4A, dotted line); the absorption at ~280 nm was almost unchanged. Reduction of RH_{stop} with H_2 yielded similar results (Fig. 4B, dotted line). The difference spectra (reduced-minus-oxidized RH, insets in Figs. 4A and B) showed two main minima (bleachings) around 410 and 550 nm, respectively.

Whereas bleaching solely around 410 nm has been observed upon reduction of [4Fe-4S] clusters (24,25), two minima as found in the RH spectrum may be attributed to the reduction of [2Fe-2S] clusters (26,27).

Characterization of Fe-S clusters by X-ray absorption spectroscopy (XAS)

By XAS (22,28) at the Fe K-edge, selectively the iron sites in the RH preparations were studied. Because the coordination of the Fe of the Ni-Fe site was similar in RH_{WT} and RH_{stop} both in the oxidized and H_2-reduced states and this Fe remained in its divalent oxidation state, any changes in the Fe XAS spectra were expected to be attributable to the putative Fe-S clusters.

The XANES spectra from both RH preparations (Fig. 5) were similar to typical spectra of Fe-S clusters (29-31). A pronounced shift of the Fe K-edge to lower energies by 1.0-1.2 eV after reduction by H_2 was observed (dotted lines). The shift was by 0.2 eV larger in the RH_{WT} (Table 3). A shift by ~0.2 eV was also evident in the pre-edge peak of the XANES spectra (Fig. 5, insets). Such spectral shifts are typical for Fe-S cluster reduction (29,31), implying that such clusters became reduced in RH_{WT} and RH_{stop} upon formation of the Ni-C state.

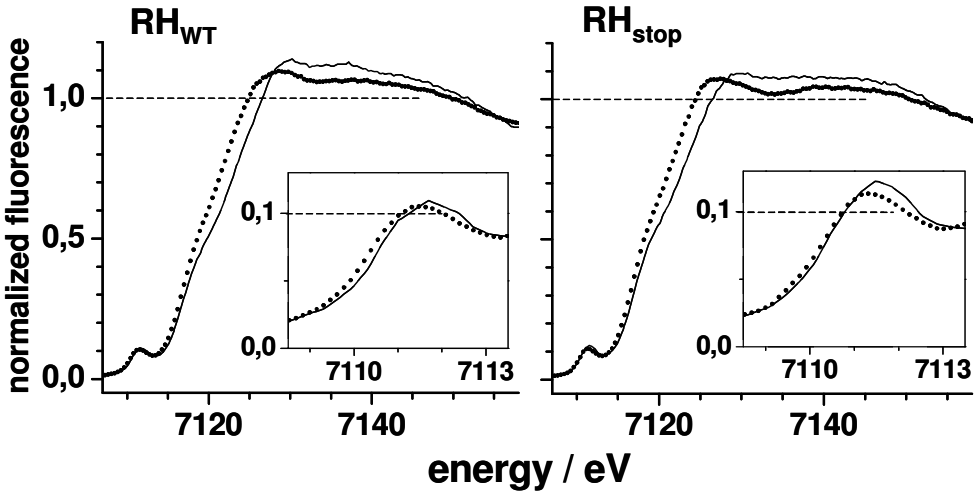

Figure 5: Normalized Fe XANES spectra of oxidized (solid lines) and H_2-reduced (dotted lines) RH preparations. The insets show the pre-edge peaks in magnification. Dashed lines emphasize the spectral differences between RH_{WT} and RH_{stop}.

The maxima of the XANES spectra of the RH_{WT} were larger and the pre-edge peak magnitudes and areas were smaller than in the RH_{stop}, pointing to an average coordination of Fe in the RH_{WT} by less sulfur and more O/N ligands (32). For one-

electron reduction of single-Fe^{III} compounds with mixed O/N/S-ligation of iron, a shift of the K-edge by about -2.5 eV may be expected (29,31,33). Hence, it was estimated that 3-4 and ~2 Fe atoms (on basis of 8 and 5 Fe atoms in total) became reduced in the $RH_{WT}^{+H_2}$ and $RH_{stop}^{+H_2}$, respectively (Table 3). In both preparations, obviously more than one electron was transferred to Fe in the Ni-C state. Moreover, the overall Fe coordination was different and additional Fe atoms seemed to become reduced in the RH_{WT}.

Table 3: Fe XANES features of RH_{WT} and RH_{stop}. E_{edge}, K-edge energy at 50 % of normalized X-ray fluorescence; ΔE_{edge}, edge shift in the H_2-reduced state.

	E_{edge} [eV] ±0.1 eV	ΔE_{edge} [eV] ±0.1 eV	K-edge maximum at 7130 eV	$E_{pre\text{-}edge\ peak}$ [eV] ±0.1 eV
RH_{WT}^{ox}	7119.9		1.14	7110.3
$RH_{WT}^{+H_2}$	7118.7	-1.2 (3.8)[a]	1.09	7110.1
RH_{stop}^{ox}	7119.3		1.09	7110.2
$RH_{stop}^{+H_2}$	7118.3	-1.0 (2.0)[a]	1.05	7110.0

[(a)]values in parenthesis are a rough estimate of the numbers of Fe ions that became reduced in the Ni-C state calculated using an edge shift ΔE_{1Fe} of -2.5 eV per single-Fe^{III} reduction, Fe contents (N_{Fe}^{RHi}) of 8 and 5 per [HoxBC] unit in RH_{WT} and RH_{stop}, and the measured edge shifts ΔE_{edge}^{RHi} according to ($N_{Fe}^{RHi} \bullet \Delta E_{edge}^{RHi}$) / ΔE_{1Fe}.

The Fourier-transforms (FTs) of Fe EXAFS oscillations (Fig. 6) of oxidized RH_{WT} and RH_{stop} showed two prominent peaks immediately revealing the presence of at least two backscatterer shells, likely due to Fe-O/N/S and Fe-Fe/Ni interactions around 2-2.2 Å and 2.7 Å (the true Fe-backscatterer distances are by about 0.4 Å larger than the reduced distances indicated in Fig. 6). The FTs of RH_{WT}^{ox} and RH_{stop}^{ox} were not identical; FT peak I was larger in RH_{stop}^{ox} and an additional shoulder was present on FT peak II in RH_{WT}^{ox} (Fig. 6, arrow).

Precise structural information was obtained from simulations of the EXAFS oscillations (Fig. 6, inset). In both preparations the EXAFS was expected to be dominated by contributions from Fe-C/N/O/S and Fe-Fe/Ni vectors in the first and second ligand spheres. The broad shoulder at lower distances on FT peak I in RH_{WT} (Fig. 6) suggested the presence of C/O/N atoms with significantly shorter distance from Fe than the S-atoms at about 2.3 Å. A first simulation where one Fe-C/O/N, one Fe-S, and one Fe-Fe/Ni vector were included yielded an error factor R_F of about 10 % for both RH_{WT} and RH_{stop} (Table 4A, fit I). The coordination number of the Fe-Fe vector $N_{Fe\text{-}Fe}$ was close to one in both cases. For the presence of two [4Fe-4S] clusters plus one [4Fe-4S] or [3Fe-4S] cluster as in standard hydrogenases, a value of $2.5 < N_{Fe\text{-}Fe} < 3$ was expected because each Fe in such clusters has three (in [4Fe-4S]) or two (in [3Fe-4S])

Fe neighbours at about 2.7 Å distance (34-36). Thus, fit I immediately suggested that the Fe EXAFS of the RH was not dominated by cubane clusters. Instead, a value of $N_{Fe\text{-}Fe}$ close to one was compatible with the predominant presence of Fe-clusters where each Fe ion has only one Fe neighbour in both RH preparations. Such a situation is realized in [2Fe-2S] clusters. That N_S was much lower than 4 suggested the mixed coordination of several Fe ions by O/N and S ligands and not predominantly by terminal Cys-S and bridging μ-S ligands as observed for [4/3Fe-4S] clusters. If [2Fe-2S] clusters were present, they could therefore be of the Rieske type ([2Fe-2S](Cys-S)$_2$(His-N)$_2$).

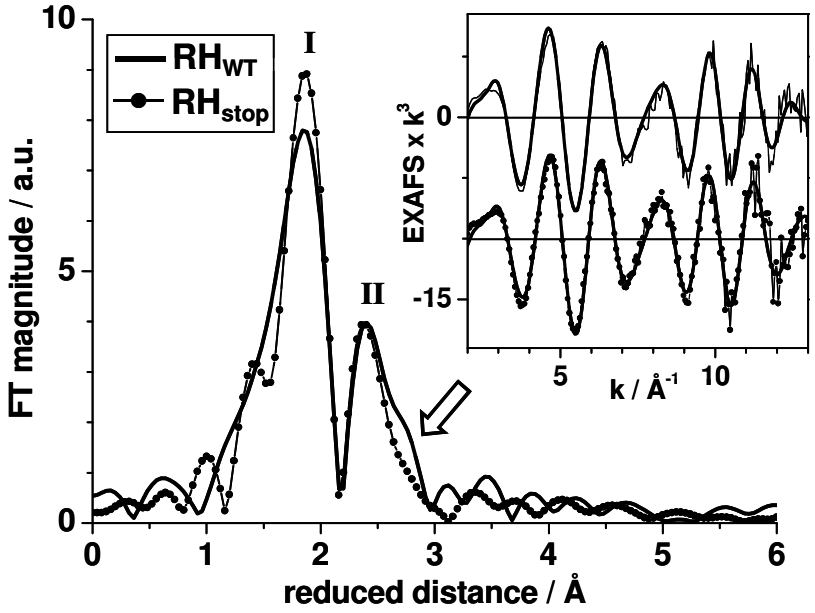

Figure 6: Fourier-transforms (FTs) of k^3-weighted Fe EXAFS oscillations (in the inset) of RH_{WT} (solid lines) and RH_{stop} (dotted lines) (thick lines in the inset: simulations according to Table 4A, fit III). Arrow: contribution to the RH_{WT} EXAFS from ~3 Å Fe-Fe interactions.

The EXAFS of RH_{WT}^{ox} showed a shoulder on FT peak II which was absent in RH_{stop}^{ox}. Inclusion of a second Fe-Fe vector in the simulations to account for this feature almost halved the R_F value for RH_{WT}^{ox} (Table 4A, fit II) whereas it did not significantly improve the fit for RH_{stop}^{ox}. Furthermore, the Debye-Waller parameters ($2\sigma^2$) were unrealistically large for both Fe-Fe vectors meaning that a distinct long Fe-Fe distance was likely not present in RH_{stop}. The estimated longer Fe-Fe distance of >3 Å in RH_{WT}^{ox} is not observed in normal [4Fe-4S], [3Fe-4S], or [2Fe-2S] clusters where typical Fe-Fe distances are ~2.7 Å (29,31,34-36). These results seemed to imply the presence of an additional more unusual Fe-cofactor in the RH_{WT}.

Table 4: Simulation results of EXAFS spectra from RH_{WT} and RH_{stop} (ox, oxidized state; H_2, Ni-C state).

(A)	shell	N_i [per Fe atom]	R_i [Å]	$2\sigma^2_i$ [Å^2]	R_F [%]
RH_{WT}^{ox} (fit I / fit II / fit III)	Fe-C	- / - / 0.11$^{\#}$	- / - / 1.95	- / - / 0.002*	9.2/ 5.4/ 5.6
	Fe-N,O	2.52 / 2.40$^{\#}$ / 2.15$^{\#}$	2.06 / 2.05 / 2.05	0.021 / 0.022 / 0.023	
	Fe-S	2.60 / 2.60$^{\#}$ / 2.74$^{\#}$	2.26 / 2.26 / 2.26	0.012 / 0.012 / 0.012	
	Fe-Fe,Ni	0.85 / 1.16 / 1.16	2.73 / 2.74 / 2.74	0.004 / 0.008§ / 0.008§	
	Fe-Fe	- / 0.46 / 0.46	- / 3.02 / 3.02	- / 0.008§ / 0.008§	
RH_{stop}^{ox} (fit I / fit II / fit III)	Fe-C	- / - / 0.51$^{\#}$	- / - / 1.90	- / - / 0.002*	9.5/ 9.1/ 6.5
	Fe-N,O	2.24 / 2.36$^{\#}$ / 1.69$^{\#}$	2.08 / 2.07 / 2.10	0.046 / 0.054 / 0.012	
	Fe-S	2.46 / 2.64$^{\#}$ / 2.80$^{\#}$	2.26 / 2.26 / 2.25	0.008 / 0.008 / 0.010	
	Fe-Fe,Ni	1.09 / 1.63 / 1.11	2.72 / 2.72 / 2.73	0.008 / 0.016§ / 0.008	
	Fe-Fe	- / 0.37 / -	- / 3.04 / -	- / 0.016§ / -	
(B) RH^{+H_2} (WT / stop)	Fe-N,O	2.28$^{\#}$ / 1.69$^{\#}$	2.13 / 2.21	0.036 / 0.015	8.5/ 10.7
	Fe-S	2.72$^{\#}$ / 3.31$^{\#}$	2.28 / 2.27	0.009 / 0.010	
	Fe-Fe,Ni	1.01 / 1.14	2.72 / 2.71	0.005 / 0.008	
(C) extra Fe in RH_{WT} (4Fe-3S-3O)[a]	Fe-N,O	1.50* (1.50)	1.99 (1.94)	0.001 (0.001)	9.8
	Fe-S	2.50* (2.50)	2.28 (2.26)	0.008 (0.007)	
	Fe-Fe	1.00* (1.00)	2.73 (2.73)	0.005 (0.006)	
	Fe-Fe	1.00* (1.00)	3.02 (3.11)	0.007 (0.004)	

N_i, coordination number; R_i, absorber-backscatterer distance; $2\sigma^2_i$, Debye-Waller parameter; R_F, error value calculated as defined in (48) over a reduced distance range of 1 to 3 Å. **(A)** Three fit approaches to spectra from oxidized enzymes; **(B)** fit of the spectra from H_2-reduced enzymes; **(C)** fit of the spectrum of the tentatively isolated contribution from the extra Fe ions in RH_{WT} (see Fig. 8) (a, values in parenthesis refer to the [4Fe-3S-3O] cluster in *D. desulfuricans* (39)). The following fit restraints were applied: $^{\#}$, the sum of $N_{1\text{-}3}$ was restricted to a value of 5.0; §, $2\sigma^2$ was coupled to yield equal values for the respective backscatterer shells; *, parameters were not varied in the simulations.

In a third simulation a C-shell was included to account for the 3 CN/CO ligands of the Fe of the Ni-Fe site. The fit for RH_{WT}^{ox} was not improved, supporting its lower (CN,CO)/Fe ratio. A significantly improved fit was obtained for RH_{stop}^{ox} (Table 4A, fit III) where the coordination number of the Fe-(CN,CO) vector was in agreement with its larger (CN,CO)/Fe ratio of ~0.6 according to the lower Fe content.

To gain more support for the unexpected result that the Fe-Fe coordination number ($N_{Fe\text{-}Fe}$) was close to one, a particularly stringent analysis (37) of the Fe-Fe vector in RH_{stop} was performed. The values of $N_{Fe\text{-}Fe}$ and $2\sigma^2_{Fe\text{-}Fe}$ were varied, an EXAFS simulation was carried out for each parameter couple, and the resulting fit errors (R_F) were depicted in Fig. 7. Clearly, the absolute minimum (R_F = 12 %) in the fit function was obtained at a value of $N_{Fe\text{-}Fe}$ close to one. The presence of only one [4Fe-4S] cluster was strongly disfavoured because at the then expected $N_{Fe\text{-}Fe}$ of 2.6 (taking into account the Fe from the Ni-Fe active site) R_F was three-fold increased. The presence of only one [3Fe-4S] or of one [2Fe-4S] plus one [3Fe-4S] in RH_{stop} was also disfavoured because at the then predicted $N_{Fe\text{-}Fe}$ values of 1.75 and 1.5 (including the single Fe-Ni vector) R_F was already about doubled (Fig. 7). Thus, the presence of two [2Fe-2S] clusters appeared to be the most likely option in RH_{stop}.

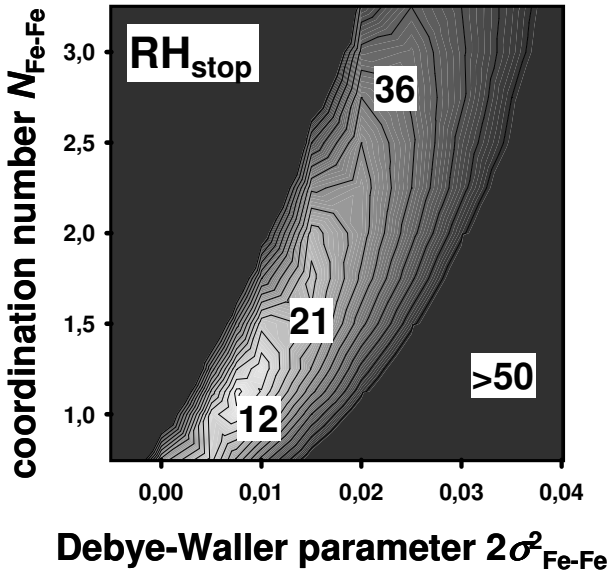

Figure 7: Contour plot of R_F values (numbers in the figure given in %) derived from two shell simulations (1x Fe-S and 1x Fe-Fe; $N_{Fe\text{-}S}$ was allowed to vary in the simulations; $2\sigma^2_S$ was restricted to positive values) of the RH_{stop}^{ox} EXAFS under variation of the coordination number ($N_{Fe\text{-}Fe}$) and Debye-Waller parameter ($2\sigma^2_{Fe\text{-}Fe}$) of the ~2.7 Å Fe-Fe vector. Contour lines are spaced by ΔR_F = 3 %. White colour denotes for lowest R_F-values (best fit).

The Fe-Fe distances in [4/3Fe-4S] clusters in crystallized Ni-Fe hydrogenases range between 2.62-2.77 Å ((34-36); unusually long (38) and short (39) Fe-Fe distances were neglected); the range is similar in [2Fe-2S] clusters (29,31). The Debye-Waller parameters of the ~2.7 Å Fe-Fe vectors corresponded to a smaller distance spread of only ~0.07 Å (Table 4A). Superimposition of EXAFS oscillations from Fe-Fe vectors differing by less than 0.1 Å does not cause significant destructive interference (22,37) rendering underestimation of $N_{Fe\text{-}Fe}$ unlikely.

In RH_{WT} the fit minimum for the ~2.7 Å Fe-Fe vector was also observed for $N_{Fe\text{-}Fe}$ ~1 irrespective of the specific fit approach, e.g. inclusion of 1-3 O/N/C ligand shells and/or of an additional ~3 Å Fe-Fe vector (not documented). Presumably, RH_{WT} contained the same [2Fe-2S] clusters as RH_{stop} and, furthermore, an additional Fe-S cluster (see below).

In the H_2-reduced state, the EXAFS spectra of both RH preparations were overall similar to the ones in Fig. 6; in particular, the shoulder on FT peak II due to long Fe-Fe distances was still present in RH_{WT}^{+H2} (data not shown). Simulations revealed significantly elongated Fe-O/N and Fe-S distances; the Fe-Fe/Ni vectors of ~2.7 Å length were slightly shortened (Table 4B). Very similar effects have been observed upon reduction of the $[2Fe\text{-}2S]^{Rieske}$ cluster in *Pseudomonas cepacia* phthalate dioxygenase (29). Fe-S cluster reduction was clearly detectable both in the XANES and EXAFS of the RH in the Ni-C state.

Tentative identification of the additional Fe-cofactor in RH_{WT}

The EXAFS of RH_{WT} revealed Fe-Fe distances of ~3 Å which were absent in RH_{stop}. Similar Fe-Fe distances were found in the [4Fe-3S-3O] cluster in the proximal position of the small subunit of the Ni-Fe hydrogenase from *Desulfovibrio desulfuricans* (36). To test the hypothesis whether the RH_{WT} may contain a [4Fe-3S-3O] cluster, a tentative isolation of the contribution of the extra Fe to the RH_{WT} EXAFS was performed (Fig. 8, see legend). The resulting EXAFS difference spectrum (from oxidized enzymes) revealed pronounced splitting of both FT peaks. (The difference from the H_2-reduced enzymes was similar (not shown).) The best fit was achieved using a $(O/N)_{1.25\text{-}1.75}S_{2.25\text{-}2.75}$ Fe-coordination and two Fe-Fe vectors with $N_{Fe\text{-}Fe}$ = 1 and ~2.7 Å and ~3 Å length (Table 4C). The [4Fe-3S-3O] cluster in *D. desulfuricans* reveals similar structural motifs (Fig. 8, inset) and also 4-coordinated Fe ions (Table 4C, in parenthesis). The FT (Fig 8, triangles) of an EXAFS spectrum calculated on basis of the crystal structure (36) was similar to the one tentatively attributed to the extra Fe-S species in RH_{WT}. The binding of one extra [4Fe-3S-3O] to each HoxB subunit was thus a conceivable option in RH_{WT}.

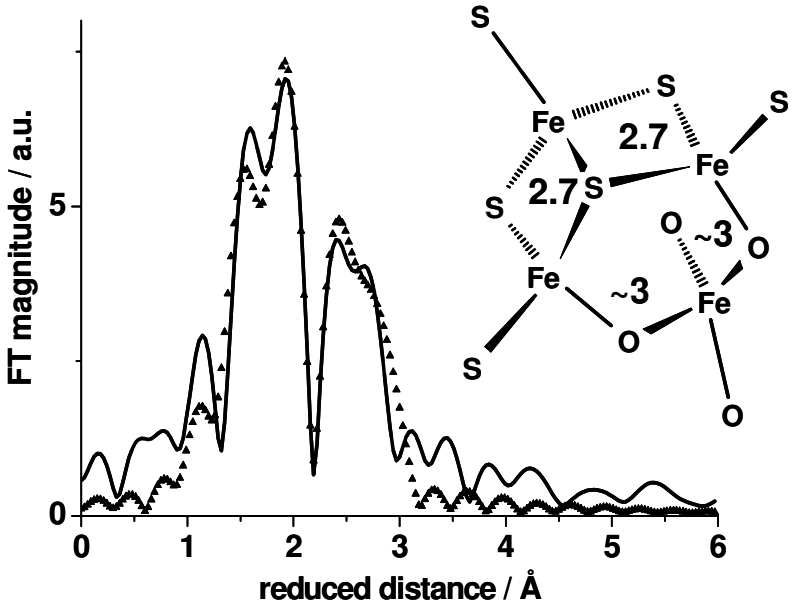

Figure 8: FT of a k^3-weighted EXAFS spectrum (solid line) tentatively attributed to the extra Fe present in RH_{WT}, but not in RH_{stop}. The FT was calculated from normalized EXAFS oscillations $\chi(k)$ representing $[(9\chi_{RH_{WT}} - 5\chi_{RH_{stop}}) / 4]$. Here, the presence of four extra Fe ions in HoxB of RH_{WT} was assumed (taking into account the error range of the Fe content, Table 1) to allow for comparison with the theoretical EXAFS spectrum (triangles) of the [4Fe-3S-3O] cluster (inset) in the *D. desulfuricans* crystal structure (39) calculated by using parameters given in Table 4C (in parenthesis).

Discussion

The RH of *R. eutropha* belongs to a subclass of Ni-Fe hydrogenases acting as hydrogen sensors (3). H_2-sensing proteins have also been examined in *B. japonicum* (7) and *R. capsulatus* (8). Moreover, genome sequencing projects of a number of microorganisms have uncovered sequences of additional potentially H_2-sensing Ni-Fe hydrogenases (Fig. 9). These proteins may all be similarly organized; the large subunit carrying a Ni-Fe site and the small subunit harbouring Fe-S clusters. However, due to the lack of crystal structures only few information about the chemical nature of the putative Fe-S clusters in the H_2-sensing hydrogenases was available. In this study, for the first time

the structure and function of Fe-S clusters in the oxygen insensitive hydrogen sensor of *R. eutropha* was investigated.

Alignment of the HoxB amino acid sequence with those of the small subunits of crystallized Ni-Fe hydrogenases and of potential H_2-sensors (Fig. 9) shows that the conserved residues coordinating the Fe ions of Fe-S clusters in standard hydrogenases are always present. Thus, on the level of amino acid primary sequences one might argue that the small subunits of H_2-sensing hydrogenases possibly contain Fe-S clusters such as found in the standard hydrogenases. Crystal structure analyses (34-36) revealed that the standard hydrogenases harbour a proximal [4Fe-4S] cluster coordinated by four cysteine residues ("P_1" to "P_4" in Fig. 9). The medial cluster usually is a [3Fe-4S] cluster coordinated by three cysteines except for the Ni-Fe-Se enzyme from *D. baculatum* (38) where a [4Fe-4S] cluster is found due to the replacement of one proline residue by another cysteine (39). All four cysteines are present in the sequences of the small subunits of the H_2 sensors ("M_1" to "M_4" in Fig. 9). The distal [4Fe-4S] cluster is coordinated by three cysteines and one histidine which are conserved in all Ni-Fe hydrogenases including the H_2 sensors ("D_1" to "D_4" in Fig. 9). One cysteine is shifted by one amino acid in the binding motif for the distal Fe-S cluster ("D_3" in Fig. 9).

In spite of these striking sequence similarities, our experimental data provided no evidence for [4Fe-4S] or [3Fe-4S] clusters in the RH, but, instead, favoured the presence of [2Fe-2S] clusters possibly of the Rieske type. These may be coordinated by two cysteines and possibly two histidines. Conserved histidine residues present only in the sequences of the H_2 sensors that could be involved in Fe-S cluster binding are highlighted in Fig. 9 ("H_1" to "H_4"). The coordination of Fe ions by non-sulfur ligands could also be explained by the oxidative conversion of cysteine thiols to sulfenates (Cys-SOH) or sulfinates (Cys-SO_2H) observed in a variety of proteins (40, 41), which would impair direct coordination of Fe ions by Cys-S. The presence of [2Fe-2S] clusters instead of [4Fe-4S] clusters in the RH may thus be related to thiol group oxidation under aerobic conditions. Preliminary Resonance Raman data suggested the presence of Fe-O bonds in RH_{stop} (I. Zebger & P. Hildebrandt, unpublished results). Thus, in RH_{stop} perhaps Fe-binding oxygens (from terminal or bridging oxidized thiol groups) may be present. Future studies will employ Mössbauer and Resonance Raman spectroscopy to elucidate further details of the Fe-S clusters of the RH. Interestingly, in the Ni-Fe hydrogenase of the aerobic *Thiobacillus ferrooxidans* only 8 Fe per Ni were found instead of the 12-13 Fe per Ni in standard Ni-Fe hydrogenases (42). Possibly, [2Fe-2S] clusters may be present in Ni-Fe hydrogenases from a variety of aerobic organisms.

Metal quantification and XAS analysis seemed to reveal an additional Fe-S cluster in RH_{WT} which is absent in RH_{stop}. In *D. desulfuricans*, a [4Fe-3S-3O] cluster is found in the proximal position (36) with Fe-Fe distances of ~3 Å as also observed in RH_{WT}. The authors postulated its formation in a reaction of a normal [4Fe-4S] cluster

with O_2 and H_2O (39) causing release of H_2S and a Fe coordination change from Cys30 to Glu87, a strictly conserved residue in the sequences of all Ni-Fe hydrogenases ("E" in Fig. 9). As the RH operates under aerobic conditions, similar [4Fe-3S-3O] cluster formation may readily occur. A [4Fe-3S-3O] cluster has also been found in the so-called "prismane" protein (43). The aerobic conversion of a [4Fe-4S] into a [4Fe-3S-3O] cluster may be a more general feature of Fe-S proteins.

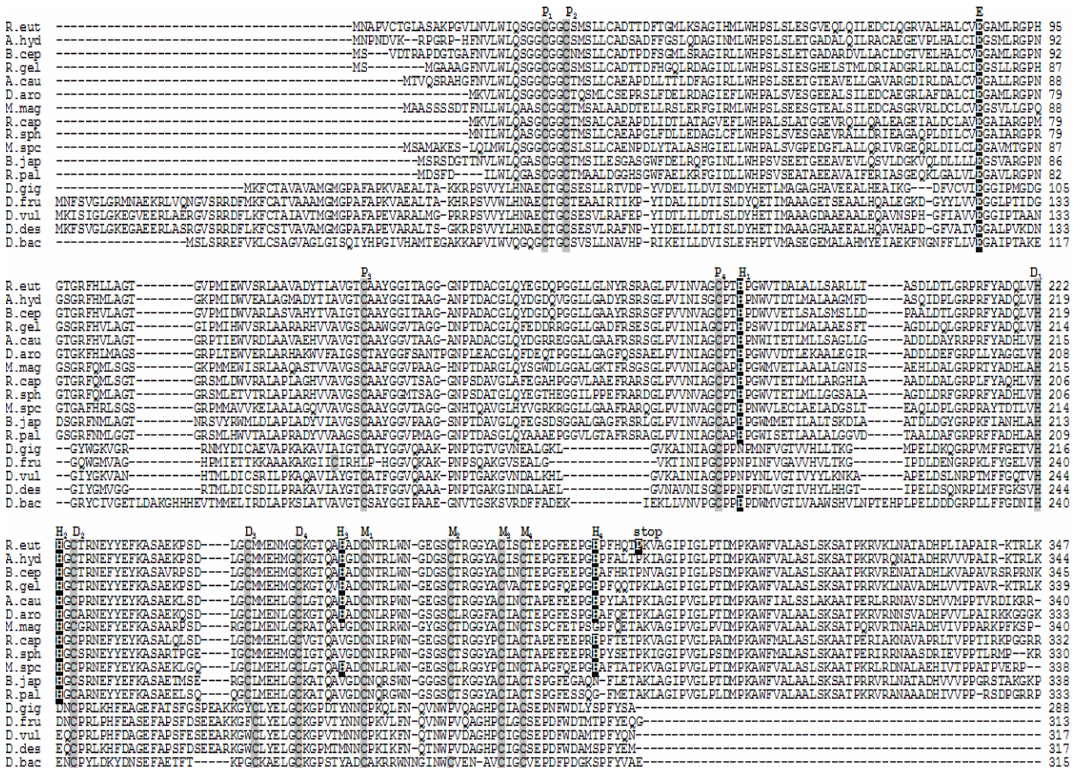

Figure 9: Alignment of the amino acid sequences of Ni-Fe hydrogenase small subunits from known and potential H_2-sensing hydrogenases from *Ralstonia eutropha* H16 (R.eut; accession number AAB49364), *Alcaligenes hydrogenophilus* (A.hyd; AAB49360), *Burkholderia cepacia* R1808 (B.cep; ZP00224364), *Rubrivivax gelatinosus* PM1 (R.gel; ZP00243688), *Azorhizobium caulinodans* (A.cau; AAS91023), *Dechloromonas aromatica* RCB (D.chl; ZP00203774), *Magnetospirillum magnetotacticum* MS-1 (M.mag; ZP00054235) *Rhodobacter capsulatus* (R.cap; AAC32032), *Rhodobacter sphaeroides* 2.4.1 (R.sph; CAA74584), *Magnotococcus spec.* MC-1 (M.spc; ZP00288962), *Bradyrhizobium japonicum* USDA110 (B.jap; AAA62627), *Rhodopseudomonas palustris* CGA009 (R.pal; CAE26403) and from the five crystallized standard Ni-Fe hydrogenases from *Desulfovibrio gigas* (D.gig; P12943), *Desulfovibrio fructosovorans* (D.fru; P18187), *Desulfovibrio vulgaris* Miyazaki F (D.vul; P21853), *Desulfovibrio desulfuricans* G20 (D.des; ZP00129917) and from the Ni-Fe-Se hydrogenase from *Desulfomicrobium baculatum* (D.bac; AAA23376). Amino acids highlighted by a grey background coordinate the Fe ions of the proximal (P_1 to P_4), the medial (M_1 to M_4) and the distal (D_1 to D_4) Fe-S cluster in the standard hydrogenases. Amino acids highlighted by a black background (H_1 to H_4; E) are discussed in the text as potential ligands to Fe-S clusters in the RH from *R. eutropha*. "stop" indicates the proline residue the codon of which has been replaced by a stop codon to generate the RH_{stop} protein.

The range of the Fe content in RH_{WT} was also compatible with the binding of only one extra Fe-S cluster per $[HoxBC]_2$ by residues from the two HoxB proteins. Such a binding mode was observed in *Rhodospirillum rubrum* dimeric CO-dehydrogenase (CODH) where a [4Fe-4S] cluster is ligated by two cysteines from each of the two CODH molecules (44). The binding of a [4Fe-3S-3O] in between two HoxB units may be less likely for symmetry reasons since this cluster should be coordinated by three cysteines and by one glutamate residue.

In RH_{stop} where the C-terminal extension of HoxB was truncated, XAS-detectable ~3 Å Fe-Fe distances were absent. The RH_{stop} protein does not form the RH double dimer $[HoxBC]_2$ and is also unable to bind the PAS domain of the HoxJ protein (14). The HoxB C-terminus may thus mediate these protein interactions and stabilize the Fe-S species appearing to be lost in RH_{stop}. Loss of a Fe-S cluster in this position in RH_{stop} could affect the Ni-Fe site in HoxC of the RH and the efficiency of electron transfer. Indeed, the Ni coordination may differ between RH_{WT} and RH_{stop} (Haumann et al., unpublished results). However, the hydrogen cleavage activity at the Ni-Fe site was unchanged. Assuming a maximal distance between the Fe-S clusters of about 25 Å as in standard hydrogenases, electron transfer between these clusters may in any event proceed at least within seconds (45).

Compared with energy generating hydrogenases the RH displays a very low but clearly defined hydrogen cleavage turnover rate (3,10). Consequently, electrons have to be released from the Ni-Fe active site. In standard Ni-Fe hydrogenases these electrons are transferred to the Fe-S clusters, which, when reduced, show typical EPR signals (1,13). In the RH, the splitting of H_2 at the Ni-Fe site yields the EPR-detectable Ni-C state (10,11), but no EPR signals from reduced Fe-S clusters in the HoxB subunit were observed. Previous UV-VIS data were interpreted to suggest reduction of a two-electron accepting organic cofactor in the RH (10). The more detailed UV-VIS analysis performed in the present study clearly indicated the reduction of Fe-S clusters upon incubation of the RH with H_2. No evidence for an additional organic redox cofactor was obtained.

In the presence of hydrogen, the reduction of Fe ions both in RH_{WT} and RH_{stop} was unambiguously detected by Fe XAS spectroscopy. In case of the RH_{stop} protein, two Fe ions possibly from two $[2Fe\text{-}2S]^+$ clusters in the medial and distal positions of HoxB seemed to become reduced. Their presumably small distance of about 12 Å may cause strong magnetic coupling between the Fe^{II} ions, rendering them EPR invisible by relaxation enhancement. In RH_{WT}, there was evidence for the reduction of up to four Fe. Thus, besides of formation of two $[2Fe\text{-}2S]^+$ clusters, the putative [4Fe-3S-3O] cluster may become doubly reduced. The [4Fe-3S-3O] cluster in "prismane" proteins was shown to exist in four oxidation states (43); the doubly reduced state was EPR silent. This cluster, however, showed a bleaching around 400 nm in the UV-VIS spectrum (46)

upon reduction similar to that of RH_{WT}. Thus, a doubly reduced [4Fe-3S-3O] cluster may also escape detection by EPR in the RH.

The sensing of H_2 involves complex formation between double dimeric RH and a tetramer of the histidine protein kinase HoxJ (14). A similar arrangement has been described in the *R. capsulatus* regulatory hydrogenase (47). In the RH, reduction of Fe-S clusters of the HoxB subunit may cause a structural change of the RH-HoxJ complex, thereby modifying its phosphorylation activity. These events may represent the first step in the signal transduction chain leading to the expression of the energy converting Ni-Fe hydrogenases in *R. eutropha*.

References

1. Cammack, R., Robson, R., and Frey, M. Eds. (1997) *Hydrogen as a fuel: Learning from nature*. Taylor & Francis, London, UK.
2. Schink, B., and Schlegel, H. G. (1978) *Biochimie* **60**, 297-305.
3. Pierik, A. J., Schmelz, M., Lenz, O., Friedrich, B., and Albracht, S. P. (1998) *FEBS Lett.* **438**, 231-235.
4. Schneider, K., Schlegel, H. G. (1976) *Biochim. Biophys. Acta* **452**, 66-80.
5. Schink, B., and Schlegel, H. G. (1979) *Biochim. Biophys. Acta* **567**, 315-324.
6. Kleihues, L., Lenz, O., Bernhard, M., Buhrke, T., and Friedrich, B. (2000) *J. Bacteriol.* **182**, 2716-2724.
7. Black, L. K., Fu, C., and Maier, R. J. (1994) *J. Bacteriol*. **176**, 7102-7106.
8. Elsen, S., Colbeau, A., Chabert, J., and Vignais, P. M. (1996) *J. Bacteriol*. **178**, 5174-5181.
9. Lenz, O., and Friedrich, B. (1998) *Proc. Natl. Acad. Sci. USA* 95, 12474-12479.
10. Bernhard, M., Buhrke, T., Bleijlevens, B., De Lacey, A. L., Fernandez, V. M., Albracht, S. P., and Friedrich, B. (2001) *J. Biol. Chem*. **276**, 15592-15597.
11. Haumann, M., Porthun, A., Buhrke, T., Liebisch, P., Meyer-Klaucke, W., Friedrich, B., and Dau, H. (2003) Biochemistry 42, 11004-11015.
12. Frey, M. (2002) Chem. Biochem. 3, 153-160.
13. Albracht, S. P. J. (1994) *Biochim. Biophys. Acta* **1188**, 167-204.
14. Buhrke, T., Lenz, O., Porthun, A., and Friedrich, B. (2004) *Mol. Microbiol*. **51**, 1677-1689.
15. Brecht, M., Van Gastel, M., Buhrke, T., Friedrich, B., and Lubitz, W. (2003) *J. Am. Chem. Soc*. **125**, 13075 - 13083.
16. Volbeda, A., Charon, M. H., Piras, C., Hatchikian, E. C., Frey, M., and Fontecilla-Camps, J. C. (1995) *Nature* **373**, 556-557.
17. Armstrong, F. A. (2004) *Curr. Opin. Chem. Biol*. **8**, 133-140.
18. Bradford, M. (1976) *Analyt Biochem* **72**, 248 - 254.

19. Klockenkämper, R. (1996) *Total Reflection X-ray Fluorescence Analysis*. Wiley, London, UK.

20. Albracht, S. P. J., van der Linden, E., and Faber, B. W. (2003) *Biochim. Biophys. Acta* **1557**, 41-49.

21. Pettifer, R. F., and Hermes, C. (1985) *J. Appl. Crystall.* **18**, 404-412.

22. Dau, H., Liebisch, P., and Haumann, M. (2003) *Anal. Bioanal. Chem.* **376**, 562-583.

23. Zabinsky, S. I., Rehr, J. J., Aukudinov, A., Albers, R. C., and Eller, M. J. (1995) *Phys. Rev. B* **52**, 2995-3009.

24. Nakamaru-Ogiso, E., Yano, T., Ohnishi, T., and Yagi, T. (2002) *J. Biol. Chem*. **277**, 1680-1688.

25. Agarwalla, S., Stroud, R. M., and Gaffney, B. J. (2004) *J. Biol. Chem*. **279**, 34123-34129.

26. Pikus, J. D., Studts, J. M., Achim, C., Kauffmann, K. E., Münck, E., Steffan, R. J., McClay, K., and Fox, B. G. (1996) Biochemistry 35, 9106-9119.

27. Kounosu, A., Li, Z., Cosper, N. J., Shokes, J. E., Scott, R. A., Imai, T., Urushiyama, A., and Iwasaki, T. (2004) J. Biol. Chem. 279, 12519-12528.

28. Yachandra, V. K. (1995) Methods Enzymol. 246, 638-678.

29. Tsang, H.-T., Batie, C. J., Ballow, D. P., and Penner-Hahn, J. E. (1989) Biochemistry 28, 7233-7240.

30. McDermott, A. E., Yachandra, V. K., Guiles, R. D., Sauer, K., and Klein, M. P. (1989) *Biochemistry* **28**, 8056-8059.

31. Cosper, N. J., Eby, D. M., Kounosu, A., Kurosawa, N., Neidle, E. L., Kurtz, D. M., Iwasaki, T., and Scott, R. A. (2002) *Prot. Sci*. **11**, 2969-2973.

32. Colpas, G. J., Maroney, M. J., Bagyinka, C., Kumar, M., Willis, W. S., Suib, S. L., Mascharak, P. K., and Baidya, N. (1991) *Inorg. Chem.* **30**, 920-928.

33. Penner-Hahn, J. E., McMurry, T. J., Renner, M., Latos-Grazynsky, L., Eble, K. S., Davis, I. M., Balch, A. L., Groves, J. T., Dawson, J. H., and Hodgson, K. O. (1983) *J. Biol. Chem*. **258**, 12761-12764.

34. Volbeda, A., Garcia, E., Piras, C., deLacey, A. L., Fernandez, V. M., Hatchikian, E. C., Frey, M., and Fontecilla-Camps, J. C. (1996) *J. Am. Chem. Soc.* **118**, 12989-12996.

35. Higuchi, Y., Ogata, H., Miki, K., Yasuoka, N., and Yagi, T. (1999) *Struct. Fold. Des*. **7**, 549-556.

36. Matias, P. M., Soares, C. M., Saraiva, L. M., Coelho, R., Morais, J., Legall, J., Carrondo, M. A. (2001) *J. Biol. Inorg. Chem.* **6**, 63-81.

37. Dau, H., Liebisch, P., and Haumann, M. (2004) *Phys. Chem. Chem. Phys*. **6**, 4781-4792.

38. Garcin, E., Vernede, X., Hatchikian, E. C., Volbeda, A., Frey, M., and Fontecilla-Camps, J. C. (1999) *Structure Fold. Des*. **7**, 557-566.

39. Rousset, M., Montet, Y., Guigliarelli, B., Forget, N., Asso, M., Bertrand, P., Fontecilla-Camps, J. C., and Hatchikian, E. C. (1998) *Proc. Natl. Acad. Sci. USA* **95**, 11625-11630.

40. Claiborne, A, Yeh, J. I., Mallett, T. C., Luba, J., Crane, E. J., Charrier, V., and Parsonage, D. (1999) *Biochemistry* **38**, 15407-15416.

41. Nagashima, S., Nakasako, M., Dohmae, N., Tsujimura, M., Takio, K., Odaka, M., Yohda, M., Kamiya, N., and Endo, I.. (1998) *Nat. Struct. Biol.* **5**, 347-351.
42. Fischer, J., Quentmeier, A., Kostka, S., Kraft, R., and Friedrich, C. G. (1996) *Arch. Microbiol.* **165**, 289-296.
43. Arendsen, A. F., Hadden, J., Card, G., McAlpine, A. S., Bailey, S., Zaitsev, V., Duke, E. H. M., Lindley, P. F., Kröckel, M., Trautwein, A. X., Feiters, M. C., Charnock, J. M., Graner, C. D., Marritt, S. J., Thomson, A. J., Kooter, I. M., Johnson, M. K., van der Berg, W. A. M., van Dongen, W. M. A. M., and Hagen, W. R. (1998) *J. Biol. Inorg.* Chem. 3, 81-95.
44. Drennan, C. L., Heo, J., Sintchak, M. D., Schreiter, E., and Ludden, P. W. (2001) Proc. Natl. Acad. Sci. USA 98, 11973-11978.
45. Moser, C. C., Keske, J. M., Warncke, K., Farid, R. S., and Dutton, P. L. (1992) Nature 355, 796-802.
46. Wolfe, M. T., Heo, J., Garavelli, J. S., and Ludden, P. W. (2002) J. Bacteriol. 184, 5 898-5902.
47. Elsen, S., Duche, O., and Colbeau A. (2003) J. Bacteriol. 185, 7111-7119.
48. Meinke, C., Sole, V. A., Pospisil, P., and Dau, H. (2000) Biochemistry 39, 7033-7040.
49. Lippard, S. J., and Berg, J. M. (1994) Principles of Bioinorganic Chemistry, University Science Books, Mill Valley, CA, USA.